Optik - International Journal for Light and Electron Optics 245 (2021) 167710

Contents lists available at ScienceDirect

Optik

journal homepage: www.elsevier.com/locate/ijleo

Original research article

Graphene-chitin bio-composite polymer based mode locker at 2 micron region

S.N.F. Zuikafly [a], H. Ahmad [b], W.M.F. Wan Nawawi [c], H. Yahaya [a], M.H. Ibrahim [d], A. A. Latif [e], F. Ahmad [a,*]

[a] Malaysia-Japan International Institute of Technology, Universiti Teknologi Malaysia, 54100 Kuala Lumpur, Malaysia
[b] Photonics Research Center, University of Malaya, 50603 Kuala Lumpur, Malaysia
[c] Department of Biotechnology Engineering, International Islamic University Malaysia, 50728 Kuala Lumpur, Malaysia
[d] School of Electrical Engineering, Faculty of Engineering, Universiti Teknologi Malaysia, 81310 Skudai, Johor, Malaysia
[e] Department of Physics, Faculty of Science, Universiti Putra Malaysia, 43400 UPM Serdang, Selangor, Malaysia

ARTICLE INFO

Keywords:
Graphene
Chitin
Mode-locker
Thulium doped fiber

ABSTRACT

In the field of pulsed fiber laser, graphene is a well-known two-dimensional (2D) material for its excellent optical properties. An alternative approach to the existing method, graphene based filament originally intended for 3-dimensional (3D) printing was used as starting material. Coupled with a newly introduced chitin nanofiber as the host polymer, it was demonstrated and reported as passive mode locker at 2-micron region. The conventional soliton operated at operating wavelength of 1982.7 nm with repetition rate of 11.35 MHz. The produced average output power, pulse width, time-bandwidth product (TBP) and signal to noise ratio (SNR) was 76.83 μW, 1.88 ps (HAC200), 0.416 and 43 dB, respectively. When the pulse was amplified with 5.4 dB of Thulium doped fiber amplifier (TDFA), the average output power increased to 3.43 mW and produced a broad operating wavelength around the 2-micron region. At the same repetition rate of 11.35 MHz, the measured pulse width, SNR, pulse energy and peak power of 7.033 ps (pulseCheck 150), 42.0 dB, 0.30 nJ, and 42.98 W, are obtained, respectively. High power laser operation in this region can find applications in medical field and sensors technology.

1. Introduction

The ever-growing industries of multiple sorts have widely used fiber lasers for their relatively high output power and design compactness. Besides its evident applications in laboratories worldwide, fiber lasers have been used for material processing such as cutting and welding [1,2], medical diagnostics [3], as well as sensor system technologies [4]. Only made possible by the use of rare-earth ions such as Ytterbium, Thulium, and Erbium as the gain mediums, fiber lasers have seen many achievements since they were first invented in 1961 [5,6].

Eye-safe region in the range of 1600–2100 nm in particular is highly sought after for its wide range of applications ranging from remote gas sensing to medical surgery [7,8]. The strong absorption lines of water particles at 2-micron region has made it expedient to applications in medical field such as laser surgery, photo dermatology and tissue ablation [9]. The newest finding of its feasible applications in the telecommunication networks made possible due to its close bandwidth ranges to that of Erbium-doped fiber's

* Corresponding author.
E-mail address: fauzan.kl@utm.my (F. Ahmad).

https://doi.org/10.1016/j.ijleo.2021.167710
Received 17 January 2021; Received in revised form 10 July 2021; Accepted 23 July 2021
Available online 30 July 2021

telecommunication wavelength [10,11] has also contributed to its increasing marketability. Research on pulsed laser generations, in particular, is still lacking in the 2-micron region compared to that of the matured telecommunication wavelength at 1.5-micron region. Laser generation through passive Q-switching technique has been utilized tremendously owing to the simplicity and flexibility in design that it can offer. Passive pulsed fiber laser generation requires a saturable absorber (SA) instead of using a bulky external control element as intra-cavity modulator. On account of this preferable prospect, many materials have been investigated as SA materials, ranging from black phosphorous, topological insulator, to metal nanoparticles [12–15].

Two-dimensional (2D) materials amongst other lower dimensional materials, despite of reports on their relatively low-damage resistance and poor long-term stability [16] had proven to be excellent materials as SAs in fiber laser generations. Recent years has shown a grown interest in the advantage of optical properties through the structural thinness offerable by 2D materials. 2D perovskite nanosheets, for example, was reported to possess stronger saturable absorption and large modulation depth as compared to its bulk counterpart [17,18]. Titanium disulphide, on another note, was also reported to possess strong light absorption properties, as well as a remarkable electrical stability making it an excellent SA material to generate pulsed laser in the telecommunication region [13]. Part of a group with broader range of bandgaps, antimonene has also gain attention for its excellent thermal conductivity and high carrier mobility. It has also been reported to be particularly excellent in optical signal processing [14]. However, these materials, while has been proven to generate ultrafast lasers in the telecommunication region, their flexibility in the medical safe wavelength are still lacking in reports. Carbon based SAs, part of the 2D materials family, in particular, have long surpassed its predecessors in regards to having lower saturation intensity, broadband operations, and speedy pulse recovery time [19,20]. Interestingly, within the carbon family, graphene was found to have a much lower saturation intensity, high carrier mobility, and greater saturable absorption when compared to that of carbon nanotubes [21], as well as higher damage threshold allowing for high power operation. In addition, the gapless linear dispersion of Dirac electrons in graphene enables tunable operation without having to physically change the graphene structure [22–24].

Graphene has been exploited in many ways in researches especially in the photonic field. Ultrafast fiber laser has seen graphene with excellent SA potentials. In investigating so, graphene has been prepared through various means to ease its integration in laser systems. Conventional method of producing graphene through mechanical exfoliation or atomic force microscopy (AFM) cantilever was reported to successfully produce few-layer graphene. Nonetheless, the graphene was still produced with ~10 nm in thickness, equivalent to 30 layer graphene [25]. Chemical vapour deposition (CVD) of graphene was first reported in an ultrafast fiber laser in 2009 [21] in which Bao et al. reported an atomic layer graphene based mode-locked fiber laser in the C-band region. Even supposing its ability to produce graphene with low defects rate and good uniformity, graphene produced through CVD and solution method was always burdened by the scrupulous yet necessary additional step of transfer process [26]. A simpler and more efficient method introduced through optical deposition of graphene instituted a more efficient and safer way of handling graphene nanostructures [21]. However, deformation- and distortion-prone characteristic of 2D materials associated with optical deposition method of SA integration was alarming. Martinez et al. [27] reported an improved performance of graphene SA through mechanical exfoliation method, a way to physically obtain multi-layered graphene, as compared to using optical deposition method, with the advantage of being simpler and having less time-consuming fabrication procedure. Nevertheless, this method is limited by the intricacies to control the size and number of layers of the produced graphene flakes. Another graphene synthesis method is the graphitization of hexagonal silicon carbide (SiC) crystals which involves high temperature of around 1500 °C as reported by Emtsev et al. which produced irregular graphene layers with wrinkled surface and restricted mobility of graphene carriers [28]. Derivatives of graphene such as graphene oxide (GO) and reduced graphene oxide (rGO) have also exhibited excellent optical properties. Unlike graphene, their hydrophilic property owing to the oxidation process of graphene can serve a wider range of researches and applications. However, the fabrication of GO and rGO involves a more complicated process and the use of hazardous material such as potassium permanganate ($KMnO_4$) requires the process to be done by an expert. Furthermore, the further reduction process of GO to produce rGO added to the complex process was proven to serve little to no effect to its performance as an SA [29].

In addition, it is found that many of the reported mode-locked lasers of carbon based SAs in the two-micron region required additional component, i.e. polarization controller (PC) to help initiate mode-locking operation. Wang et al. [30] reported a CVD graphene grown on copper foils based SA in a mode-locked laser yielding a shortest pulse width of 3.8 ns with the aid of a narrow-band fiber Bragg grating and a PC. GO based mode-locker in the 2 μm region was also reported oscillating at 1920.8 nm with a pulse duration of 1.14 ps [31]. Ahmad et al. [32] reported an rGO and titanium dioxide (TiO_2) based SA to produce a soliton mode-locking by evanescent field interaction and PC adjustment. A carbon nanotube film based SA with a high pulse energy of 26.8 nJ was reported by Wang et al. [33]. The ring cavity employed two PCs to aid the mode-locking operation of the laser. This work demonstrated a soliton mode-locking based on a graphene-chitin SA with comparable shortest pulse width and high output power as compared to similar works using carbon based materials as SAs. The soliton was also yielded at a significantly lower pump power, with high stability. Sharbirin et al. [34] reported a mode-locked thulium doped fiber laser (TDFL) using Mach-Zehnder interferometric filter at a much higher threshold input pump power of 150.4 mW.

Graphene as SAs has been prepared by mixing it in a host polymer matrix for easier in-cavity integration. Researchers have often opted for polyvinyl alcohol (PVA) in SA fabrication procedures [35–38]. As compared to other synthetic polymer such as polyethylene oxide (PEO), PVA has a higher melting point of around 180 °C [39] which is vital in pulsed laser generation. Besides PVA and PEO, polymethylmethacrylate (PMMA), polystyrene (PS) and polycarbonate (PC) among many others have been used with the same purpose. CVD graphene on PMMA as SA has been reported to produce mode-locked lasing operation with 1.2 ps pulses [40]. Despite the many choices of polymers on the market, PVA and cellulose derivatives are preferred for their affinity towards concentrated graphene aqueous solution which is better for optical density with lower non-saturable absorption losses [41]. A graphene in PVA host polymer was reported to yield a mode-locked Thulium-Ytterbium do-coped fiber laser (TYDFL) with pulse width and pulse energy of 52.85 ps

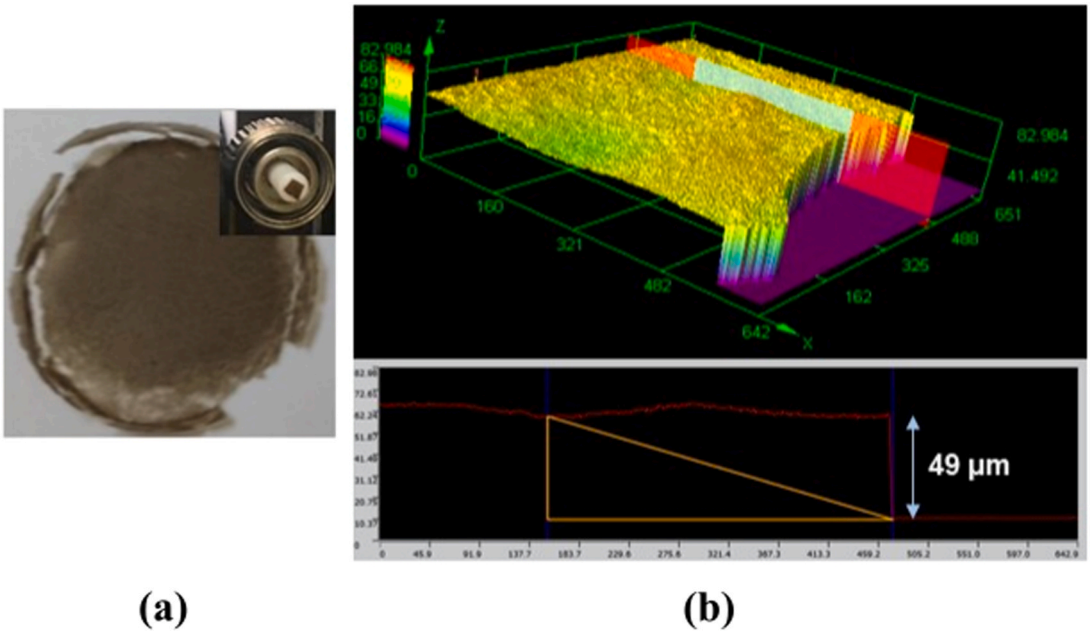

Fig. 1. (a) peeled graphene-chitin film with inset: graphene-chitin attached to the end of fiber ferrule, and (b) thickness measurement.

and 1190.5 pJ, respectively [42]. Another was reported by Zhang et al., [43] producing a repetition rate and output power of 6.46 MHz and 2 mW, respectively.

Chitin nanofiber (ChNF), fabricated from chitin, an alternative bio-host polymer is newly introduced in this work. Chitin $(C_8H_{13}O_5N)_n$ was first discovered in 1811 [44], and has since been used for many applications such as in medicine, manufacturing industries, and wastewater treatment [44,45]. ChFN was derived from the fungal origin and more hydrophobic due to its acetylated nature. This can help in hydrophobic graphene distribution (minimize agglomeration) and made percolation network already possible in minimal graphene concentration. Other than that, ChFN is resistant and durable towards higher acidity and harmful environment, making it practical for the production of films to use in a higher power and temperature laser operations, a solution of which current SA is facing where the performance of the SA is limited by their host polymers lower heat resistance. With this advantage, chitin is used in the SA fabrication process to produce a graphene-ChNF based SA for pulsed laser generation. In telecommunication applications specifically, a polymer with C-F overtones with low absorption losses at the desired wavelength is better in terms of stability [41]. This biological based material is chosen as an alternative to current conventional synthetic host polymers due to its competitive production cost, non-toxicity, water solubility, compatibility with nanomaterials, biodegradability and bioadsorbability [46]. Produced from natural resources such as plants and shells, large scale production of ChNF at low cost is highly feasible. Although chitin is no stranger in agricultural, material, and biomedical research, optical communication [47–49] has not dipped its toes into this novel material until recently when we first reported its use in the generation of a Q-switched pulsed fiber laser in the 1.5 μm region [50].

In this work, ChNF has been applied as host polymer to produce graphene based SA to produce a mode-locking operation in the 2.0 μm region. The ChNF was derived from mushrooms and combined with graphene based 3D printer filament. The TDFL yielded a lasing operation with a repetition rate and pulse width of 11.35 MHz and 7.033 ps, respectively. A high peak power was also obtained at 42.95 W. The use of ChNF in this work will contribute to a more sustainable and environmental friendly option for host polymer materials, especially in the optical communication research field.

2. Material preparations

The graphene used in the SA fabrication was obtained using a commercially available conductive graphene polylactic acid (PLA) filament which is marketed for 3D printing purposes (https://www.blackmagic3d.com/) with composition (weight %) of Graphene Platelets (30–40%), Polylactic acid (25–35%), Tris(nonylphenyl) phosphite (TNNP)(5–10%) and carbon fibers (5–10%). The graphene-PLA based filament is in black color with volume resistivity of 0.6 ohm-cm, diameter of 1.75 mm and size: 100 g, was used as per received. In order to reduce the fabrication time, the filament was extruded through a 3D printer nozzle of 0.4 mm at 210 °C to melt the plastic additive and to reduce the diameter of the filament to 400 μm. This was to ensure the graphene filament can be easily dissolved in the next step. The 25 mg weighed extruded filament was then mixed with 1 mL of tetrahydrofuran (THF). This allows for plastic component on the filament, the PLA, to dissolve thus disintegrating the graphene component, producing graphene in THF suspension. An even dispersion of the graphene-THF suspension was ascertained through a 20 min of ultrasonic bath.

The host polymer, chitin nanofiber (chitin), was prepared as per reported in [51] through the extraction of oyster mushrooms (*Pleurotus Ostreatus*). The mushrooms were blended for 5 min before undergoing hot water extraction at 85 °C. After 30 min, the

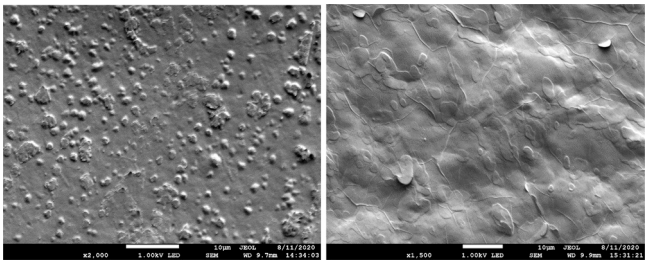

Fig. 2. FESEM image of the (a) standalone chitin and (b) fabricated graphene-chitin SA.

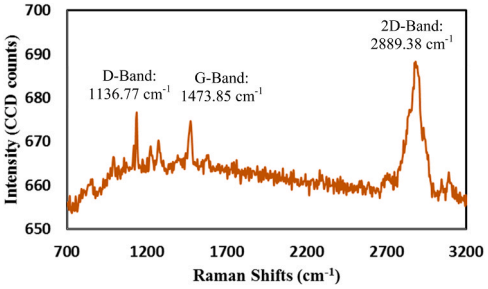

Fig. 3. Raman spectrum of the graphene-chitin SA.

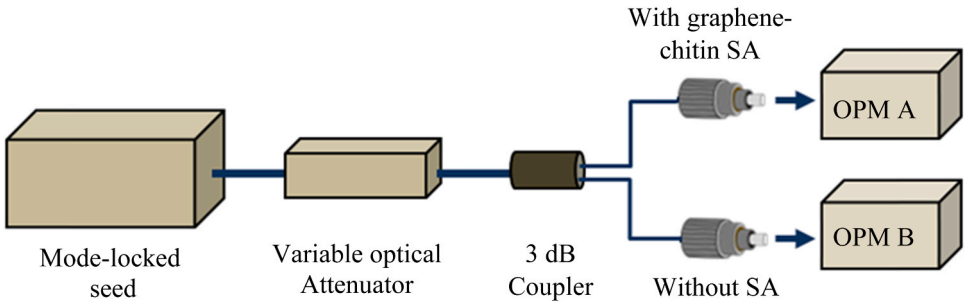

Fig. 4. Twin-balanced detector measurement setup.

mushroom tissue underwent alkali treatment (1 M NaOH) at 65 °C for three h. The extracted tissues were diluted to 0.8% w/v concentration and kept stable in diluted state at 4 °C until further use.

Consecutively, the graphene filament suspension was mixed with the chitin in 1:1 ratio. The mixture was placed in an ultrasonic bath for 1 h to ensure even dispersion of graphene in the biopolymer matrices. Then, 5 mL of the graphene in the biopolymer matrices was poured in a circular shape plastic petri dish with diameter of 32 mm and 10 mm height, and left to dry in ambient temperature for 36 h, producing a free standing graphene-chitin film SA as shown in Fig. 1(a). The thickness measurement as shown in Fig. 1(b) was done using a 3D measuring laser microscope (Olympus, LEXT OLS4100). The uniform cross section at the red-highlighted section at which the average height was measured is shown in Fig. 1(b). The height indicated in the figure depicted the film thickness, which was recorded at around 49 μm.

3. Material characterizations

The fabricated graphene-chitin SA was characterized using Raman spectroscopy (Renishaw, inVia) and Field Emission Scanning Electron Microscopy (FESEM) (JEOL, JSM-7800 F). Fig. 2 shows the surface morphology and dispersion state of the graphene-chitin based SA. The structural shape of the material that made up the sample, such as in porous, tubes, flakes or other forms can be observed here. In this case, it is believed that the graphene existed in particle form and was well dispersed in the chitin polymer matrices. In Fig. 2(a), the agglomeration of the fibrous nature of chitin can be seen as a result of the chitin drying process and comparing it to the graphene-chitin film in Fig. 2(b), it can be seen that the flake-like structure is caused by the chitin itself. No visible separation of the graphene and the chitin host polymer is visible from the FESEM image, indicating that graphene is well-dispersed. Higher accelerating voltage could be applied to get a more detailed image of the graphene particle but it is found that the charging effect affected the

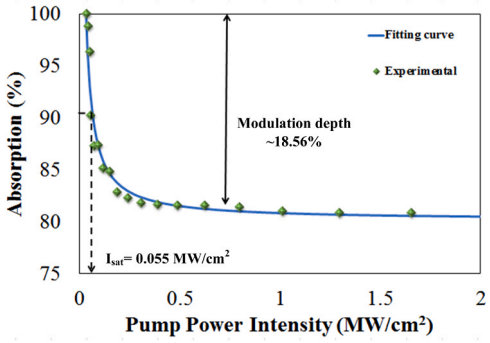

Fig. 5. Modulation depth of graphene-chitin SA.

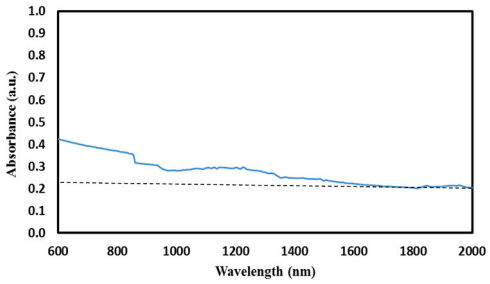

Fig. 6. UV-Vis-NIR absorption spectrum of graphene-chitin.

quality of the image at this point. The FESEM image also shows that the fabrication process was free of any surfactants that can negatively affect the non-saturable loss of the SA. Additionally, no air holes or bubbles were observed indicating a good uniformity of the fabricated graphene filament based film. The SA exhibited an eminent Raman peaks at around 1473.85 cm^{-1}, 1136.77 cm^{-1}, and 2889.38 cm^{-1} of G-band and D-band, respectively, with I_D/I_G ratio of approximately 1.0 as shown in Fig. 3. The ratio of I_{2D}/I_G was around 1.02 indicating a multilayer graphene [52]. Both bands agree to the defining Raman features of pristine graphene [53].

A twin-balanced detector setup as illustrated in Fig. 4 was used to measure the nonlinear optical response of the graphene-chitin SA. The mode-locked seed was sourced from a 1950 nm Toptica (FemtoFErb) femtosecond laser with pulse width and repetition rate of 100 fs and 30 Mhz, respectively. The mode-locked laser source was connected to a variable attenuator after which its beam is split through a 3 dB optical coupler. One of the two port of the 3 dB coupler is then connected to the graphene-chitin SA and another, directly to the optical power meter (OPM) to act as the reference port.

The output powers from the detectors with and without the graphene-chitin SA was recorded through OPMs as the attenuation value was decreased gradually.

The absorption rate was then calculated and fitted using the following equation [54],

$$Absorption \quad rate, \quad \alpha(I) = \left[\frac{\alpha_s}{1 + \frac{I}{I_{sat}}} + \quad \alpha_{ns} \right]$$

where α(I) is the absorption rate, α_s is the modulation depth, I is the input intensity, I_{sat} is the saturation current and α_{ns} is the non-saturable absorption.

As shown in Fig. 5, the measured modulation depth of the SA at 2-micron region was approximately 18.56% though a higher value is attainable with increased graphene raw material during fabrication process with the expense of higher saturable losses. However, with multi-layered graphene knowingly reported for its low modulation depths [55,56], the obtained value is considered high. The saturation intensity was measured at 0.055 MW/cm^2 with a calculated non-saturable loss of around 81%. Aside from the structure of the graphene-chitin SA itself, the low saturation intensity may be affected by the recombination time, pump pulse shape and pulse duration owing to the twin detector technique used for nonlinear measurement [57].

Fig. 6 shows the UV–vis–NIR absorption spectrum of the fabricated graphene-chitin film composite. The characterization was performed by using a Perkin-Elmer Lambda 750 UV-Vis-NIR spectrometer with 5 nm data interval. The maximum absorption of 21% was recorded at 2000 nm, indicating graphene with an approximate of 9 layers which agrees with the Raman's I_{2D}/I_G ratio. Visible absorption can be observed throughout the short wave infrared region thanks to the zero bandgap property of graphene which contributed to its wideband absorption ability. The steady and continuous absorption of maximum 42% throughout the near infrared region was higher that several reported absorptions of graphene based SAs [58–60].

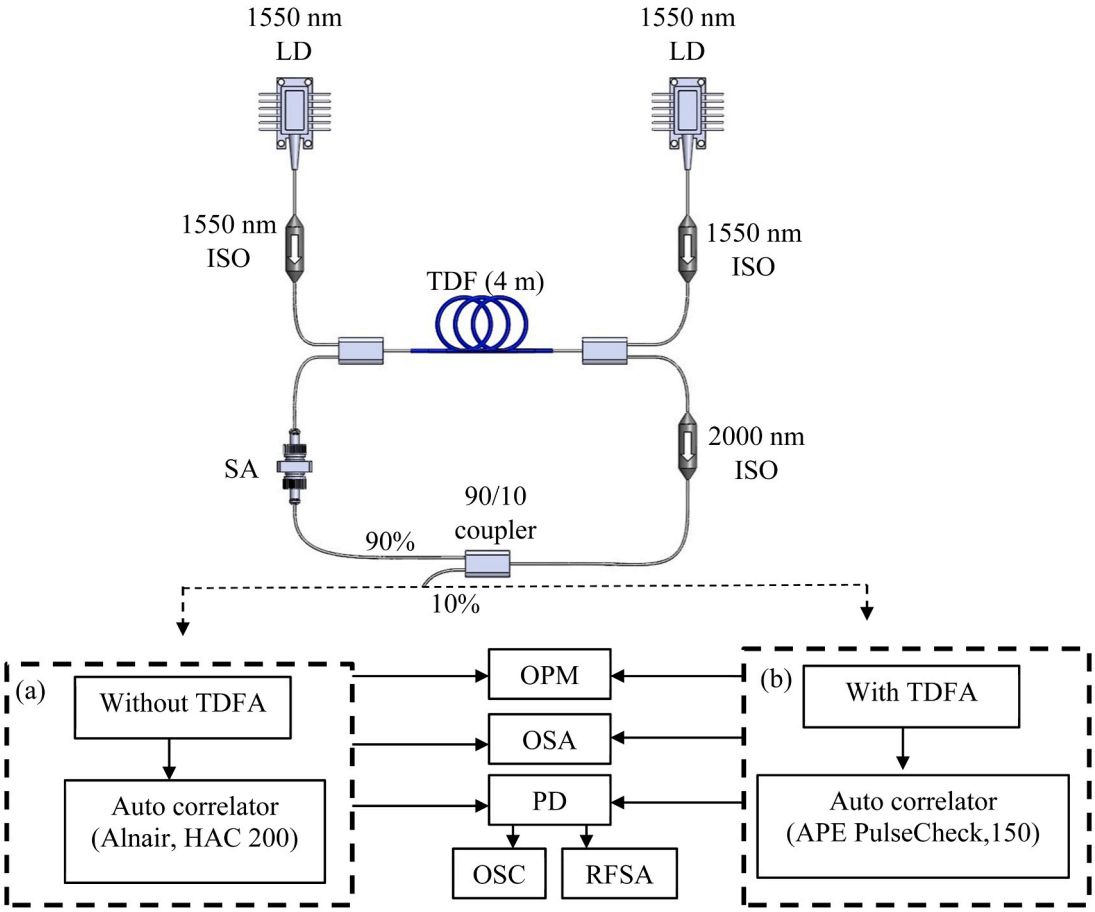

Fig. 7. Experimental setup of the mode-locked TDFL.

4. Experimental setup

Fig. 7 shows the experimental setup for the mode locked TDFL using graphene-chitin. The setup in Fig. 7 represents two variations of the same setup, in which a thulium doped fiber amplifier (TDFA) as shown in Fig. 7(b) was introduced in the latter part of the experiment in order to obtain a higher output power. The higher output power allows for the measurement of pulse width using a 2-micron autocorrelator (pulseCheck 150).

The all fiberized TDFL was configured in a ring cavity to ensure continuous light oscillations. The cavity was pumped from a pair of 1550 nm laser diode (LD) in forward pumping configuration. Besides allowing for a higher power output [61], the pumping scheme at 1550 nm at the gain medium enabled for a shorter cavity length due to the lower chance of signal reabsorption [62]. This is particularly consequential to mode-locking operations [63]. A 90/10 optical output coupler was also placed after a 2000 nm isolator in the laser cavity to keep 90% of light oscillating while the 10% of the signal was used for optical measurements. The SA was integrated in the cavity by interposing a small cut (2 mm $\times$ 2 mm) of the fabricated graphene-chitin film in between the fiber ferrules of 2.5 mm in diameter via a fiber connector. The output signal was measured through an optical spectrum analyzer (OSA)(Yokogawa AQ6375), an oscilloscope (OSC) (Rohde&Schwarz RTM3002), a radio frequency spectrum analyzer (RFSA) (Rohde&Schwarz FPC1000), and an optical power meter (OPM) for its wavelength distribution, temporal analysis, signal-to-noise (SNR) ratio, and output power, respectively. An 818-BB-51 F Newport InGaAs based 12.5 GHz photodetector was also used to allow for the conversion of optical to electrical signal when using the OSC and RFSA.

The low peak power obtained, as discussed later, was typical in picosecond pulse train. A higher gain in order to increase the laser's output power can be procured without the risk of uncurbed gain narrowing [64]. In order to measure the pulse width by using 2-micron autocorrelator (pulseCheck 150) a TDFA (Keopsys) was incorporated in the laser cavity to amplify the signal. By inserting the amplifier in the fiber laser cavity, the signal was amplified to 5.4 dBm resulting in enhanced output power of 3.43 mW.

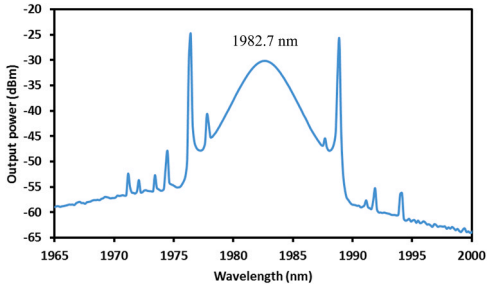

Fig. 8. Conventional soliton spectrum at the mode-locked TDFL.

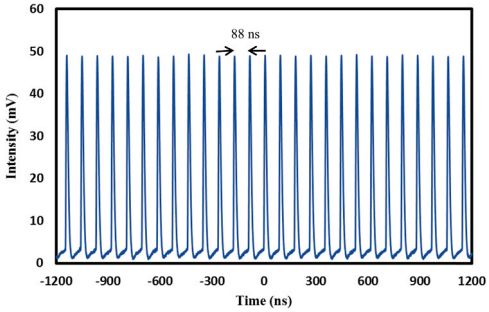

Fig. 9. Pulse train repetition rate of conventional soliton.

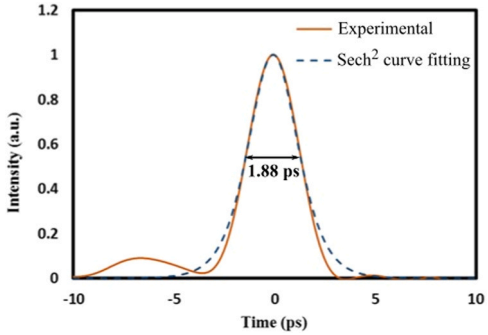

Fig. 10. Autocorrelation trace of the 1.88 ps pulse using HAC 200 autocorrelator.

5. Results and discussions

5.1. Mode-locked TDFL

The mode-locking operation of the thulium-doped laser self-started at the pump power of 76.2 mW. The operating spectrum of the mode-locked TDFL is as shown in Fig. 8. The laser operated at 1982.7 nm with an output power of −30.1 dBm and a 3 dB spectral bandwidth of approximately 2.9 nm. Two pairs of Kelly sidebands can be observed at the shoulder of the soliton mode-locked spectra indicating laser operation in an anomalous dispersion regime. These bands formation is mainly due to the linear effect perturbation of the cavity's anomalous group delay dispersion (GDD) as well as the nonlinear effect of the self-phase modulation (SPM) [65]. The change in the soliton's phase and dispersive wave at certain wavelengths then caused the formation of the sidebands [66]. The asymmetrical Kelly sidebands are attributed to the effect of four-wave mixing (FWM) in the resonant fiber laser cavity [66,67] contributing to the strong CW background while other work had also reported of such case correlating it to the nonchirped zero frequency pulse [68]. This soliton mode-locked operation is managed solely by the modulation of resonator loss by the SA itself, dissimilar to a vector soliton [69] in which an addition of a polarization controller is needed to create a 'noise-like' pulses containing combinations of multiple pulse components with various pulse width and intensity [64]. These sidebands can cause instabilities causing a negligible spike in CW. However in the case of its operation being too close to the wavelength range where the laser is above threshold, it could cause exaggerated jump in pulse energy. A recent report by Wang et al., demonstrated the use of nonlinear Fourier

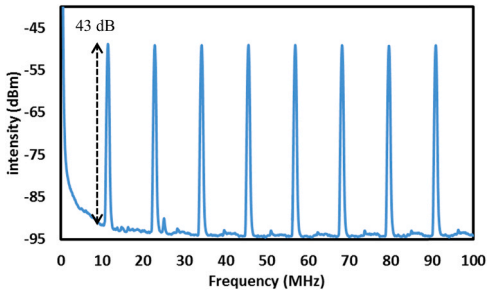

Fig. 11. Signal to noise ratio of the conventional soliton.

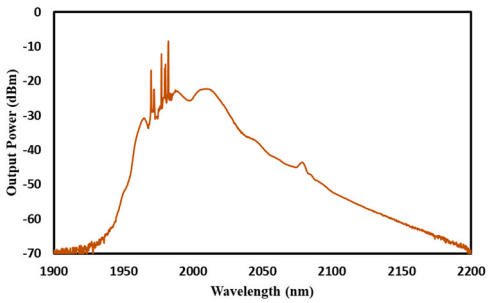

Fig. 12. OSA trace of amplified pulsed by TDFA.

transform to separate the resonant CW background which helped in obtaining pure solitons [67].

The output pulse train was recorded in Fig. 9 with pulse-to-pulse separation of 88 ns corresponding to 11.35 MHz of repetition rate. The repetition rate agrees with the overall cavity round trip length of around 18 m. The slight amplitude modulation is due to the competition between the longitudinal mode-locked supermodes which were not able to be phase locked [70]. Aside from the mode-locked regime obtained in this experiment, we did observe potential Q-switching operation but the lasing was too unstable to be recorded. This is attributed to the phase locking phenomenon of different modes of frequencies occurring as the light incident on the SA material. Q-switching instabilities are due to the difference between the decay rate of the cavity's population inversion and the field envelope which causes low frequency of relaxation oscillation [71]. Proper calculation of the laser and resonator parameter can aid in eliminating or significantly reducing if the Q-switching instabilities are found to be unwanted [72].

The generated average output power was around 76.83 μW, which was low resulting in immeasurable pulse width when using 2-micron autocorrelator (pulse check150) which requires the minimum average output power of 1 mW. As an alternative, the pulse width was measured using HAC 200 (Alnair) autocorrelator. Fig. 10 displays the second harmonic generation (SHG) autocorrelation trace (HAC 200, Alnair), with the τ_{FWHM} of 2.91 ps which resulted in the calculated pulse width of 1.88 ps (τ_{FWHM}/1.54), comparable to the reported works by Sobon et al. [40] and Yang et al. [73] in which both yielded 1.2 ps, when using CVD graphene and graphene on microfiber, respectively, and better than other reported mode-locked in the 2.0 μm region [65,74,75]. However, our pulse is not transform-limited. The $sech^2$ fitting indicating the generation of the soliton pulse is also included in the figure. The autocorrelation trace revealed that the experimental result followed the $sech^2$ fitting closely, with accompanying satellite pulse due to the nonlinearity effect in the laser cavity which has also been reported in a mode-locking based on copper oxide [76]. The calculated time-bandwidth product (TBP) was around 0.416, close to the expected transform limited value of 0.315 which is the standard temporal profile of $sech^2$ pulses. The calculated TBP indicated the existence of chirp pulses. Due to weak absorption characteristic of graphene due to its low modulation depth, graphene has limited applications in specific wavelength while facing difficulties in generating ultrashort pulses, explaining the lack of reported works on mode-locked graphene in the 2-micron region [77]. However, this work reported a graphene based SA with a more desirable modulation depth, producing short pulse duration, despite the additional non-saturation loss. The measured pulse energy and peak power is 6.7 pJ and 3.56 W, respectively.

Fig. 11 shows the radio frequency spectrum analyser (RFSA) trace for signal to noise ratio measurement with the span of 100 MHz. The recorded first beat note of SNR at 11.35 MHz was around 43 dB without any intensity fluctuation up to 7th harmonics. The obtained value of the SNR is quiet low if compared to other reported SNR for graphene based SA for two micron application such as 50 dB, 61 dB, and 50 dB [78–80]. The first contributing factor is the starting material of conductive Graphene PLA filament, which consist of 30–40 wt percent of Graphene platelets, which can be considered as multi layers graphene. The multi-layer graphene absorb more percentage of light compared to single layer or dual layers graphene, thus lower SNR value. Another factor is directly correlated to the low optical power which impinged the photodiode which causes the conversion of current to voltage to be done with some reverse bias. Despite the lower SNR value as compared to other mode-locked operation in the same region, the generated pulse was stable with very low noise level, requiring no averaging of the signal bandwidth. Higher than the minimum 30 dB is an indicator of a

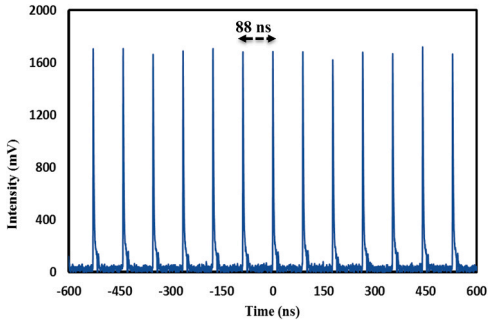

Fig. 13. Pulse train repetition rate of mode-locked soliton after TDFA insertion.

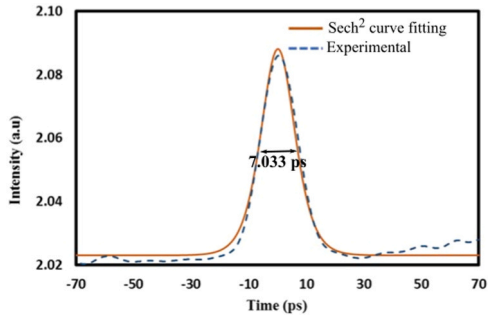

Fig. 14. Autocorrelator trace of the mode-locked TDFL using pulseCheck 150.

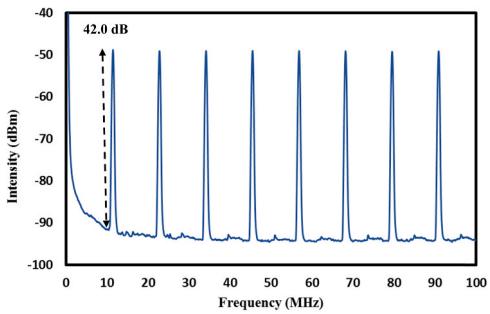

Fig. 15. SNR of mode-locked soliton after TDFA insertion.

stable pulse, since it means that the signal obtained is at least 1000 times stronger than the noise [81], the pulsed laser generation is also tested for its long term stability for an hour, showing no major fluctuation.

5.2. *Mode-locked TDFL with TDFA*

The insertion of the TDFA in the laser cavity is to increase the output power in order to use the designated autocorrelator for 2-micron region which is pulseCheck 150 (APE) autocorrelator. The autocorrelation trace of the 1.88 ps pulse for laser cavity without TDFA is carried out by using HAC 200 (Alnair) autocorrelator which is basically designed for wavelength operation at 1.5 μm. The generated average output power from the laser cavity without TDFA was around 76.83 μW, less than the minimum input power required to operate the pulseCheck 150 (APE) autocorrelator which is around 1 mW. This step is to justify the data collected during the experimental works is by using the appropriate equipment.

By inserting the TDFA, the pulse was amplified with 5.4 dB of TDFA, increasing the average output power to 3.43 mW. The resulting soliton formation is as shown in Fig. 12 where considerable loss can be seen from the wavelength shifting of the soliton with the −3 dB spectral bandwidth of 20.4 nm and the parasitic bands with broadened spectra. In spite of the additional equipment (TDFA) used, the mode-locked pulse train was kept stable with slight pulse shape modification, as shown in Fig. 13. The recorded pulse separation was at 88 ns, same as the pulse separation without TDFA, due to energy quantization.

The pulse width was then measured using a pulseCheck 150 USB second harmonic generation (SHG)-based autocorrelator. The

$sech^2$ profile in Fig. 14 indicated a pulse width of 7.033 ps. The stability of the mode-locked operation was slightly increased to an SNR ratio of 42.0 dB as depicted in Fig. 15. The measured pulse energy and peak power were at 0.30 nJ and 42.98 W, respectively.

6. Conclusion

A mode-locked thulium-doped fiber laser based on a passive SA is demonstrated. A 3D printer filament was successfully composited with a chitin based bio-polymer and fabricated into a saturable absorber. The graphene in chitin SA successfully produced a lasing scheme with a stable pulse train at 11.35 MHz with the measured pulse of 1.88 ps without TDFA and 7.033 ps of amplifies pulse with insertion of TDFA. The proposed mode-locked pulsed laser in the 2-micron region can find copious use in high precision applications especially in medicine and biomedical applications, while the use of a naturally derived host polymer can prove beneficial, environmental-wise.

Declaration of Competing Interest

The authors declare that they have no known competing financial interests or personal relationships that could have appeared to influence the work reported in this paper.

Acknowledgements

This work was supported by the Universiti Teknologi Malaysia (UTM) under UTM High Impact Reseach Grant [UTMHR, 2243.08G99]. We thank our colleagues from Photonics Research Centre, University of Malaya, who provided insight and expertise that greatly assisted the research.

References

[1] E. Beyer, A. Mahrle, M. Lutke, J. Standfuss, F. Brueckner, 2012. Innovation in high power fiber laser applications. Proceedings of SPIE, 8237, 823717.
[2] V. Kujanp, Review study on remote laser welding with fiber lasers, J. Laser Appl. 25 (5) (2014).
[3] S. Taccheo, 2017. Fiber laser for medical diagnostics and treatments: state of the art, challenges and future perspectives. Proceedings of SPIE 10058, Optical Fibers and Sensors for Medical Diagnostics and Treatment Applications XVII, 1005808.
[4] T.B. Pham, H. Bui, H.T. Le, V.H. Pham, Characteristics of the fiber laser sensor system based on etched-bragg grating sensing probe for determination of the low nitrate concentration in water, Sensors 17 (1) (2017) 1–9.
[5] A. Bellemare, A broadly tunable erbium-doped fiber ring laser: experimentation and modeling, IEEE J. Sel. Top. Quantum Electron. 7 (1) (2001) 22–29.
[6] E. Snitzer, Optical maser action of Nd^{+3} in a barium crown glass, Phys. Rev. Lett. 7 (12) (1961) 444–446.
[7] K. Bremer, A. Pal, S. Yao, E. Lewis, R. Sen, T. Sun, k T.V. Grattan, Sensitive detection of CO_2 implementing tunable thulium-doped all-fiber laser, Appl. Opt. 52 (2013) 3957–3963.
[8] L.A. Hardy, V. Vinnichenko, N.M. Fried, High power holmium: YAG versus thulium laser treatment of kidney stones in dusting mode: ablation rate and fragment size studies, Lasers Surg. Med. (2019) 51.
[9] Z. Wang, B. Zhang, J. Liu, Y. Song, H. Zhang, Recent developments in mid-infrared fiber lasers: status and challenges, Opt. Laser Technol. 132 (2020), 106497.
[10] Z. Li, A.M. Heidt, J.M.O. Daniel, Y. Jung, S.U. Alam, D.J. Richardson, Thulium-doped fiber amplifier for optical communications at 2 μm, Opt. Express 21 (2013) 9289–9297.
[11] M.H.A.K. Khushik, C. Jiang, Thulium-doped fiber amplifier for blue light signal amplification, China Commun. 16 (2019) 181–188.
[12] H. Ahmad, N.A. Hassan, S.N. Aidit, S.I. Ooi, S.W. Harun, Z.C. Tiu, Q-switching pulse generation using black phosphorus tape saturable absorber, Optoelectron. Adv. Mater. Rapid Commun. 11 (2017) 1–6.
[13] Y. Ge, Z. Zhu, Y. Xu, Y. Chen, S. Chen, Z. Liang, Y. Song, Y. Zou, H. Zeng, Z. Xu, H. Zhang, D. Fan, Broadband nonlinear photoresponse of 2D TiS_2 for ultrashort pulse generation and all-optical thresholding devices, Adv. Opt. Mater. 6 (4) (2017), 170116.
[14] Y. Song, Z. Liang, X. Jiang, Y. Chen, Z. Li, L. Lu, Y. Ge, K. Wang, J. Zheng, Z. Lu, Few-layer antimonene decorated microfiber: ultra-short pulse generation and all-optical thresholding with enhanced long term stability, 2D Mater. 4 (4) (2017), 045010.
[15] R.Z.R. Rosdin, M.T. Ahmad, Z. Jusoh, H. Arof, S.W. Harun, All-fiber Q-switched fiber laser based on silver nanoparticles saturable absorber, Dig. J. Nanomater. Biostr. 13 (2018) 1159–1164.
[16] T. Jiang, K. Yin, C. Wang, J. Hou, H. Ouyang, R. Miao, C. Zhang, K. Wei, H. Li, H. Chen, R. Zhang, X. Zheng, Z. Xu, X. Cheng, H. Zhang, Ultrafast fiber lasers mode-locked by two-dimensional materials: review and prospect, Photonics Res. 8 (1) (2020) 78.
[17] P. Li, Y. Chen, T. Yang, Z. Wang, H. Lin, Y. Xu, L. Li, H. Mu, B.N. Shivananju, Y. Zhang, Q. Zhang, A. Pan, S. Li, D. Tang, B. Jia, H. Zhang, Q. Bao, Two-dimensional $CH_3NH_3PbI_3$ perovskite nanosheets for ultrafast pulsed fiber lasers, ACS Appl. Mater. Interfaces 9 (14) (2017) 12759–12765.
[18] Y. Zhang, C.K. Lim, Z. Dai, G. Yu, J.W. Haus, H. Zhang, P.N. Prasad, Photonics and optoelectronics using nano-structured hybrid perovskite media and their optical cavities, Phys. Rep. 795 (2019) 1–51.
[19] V. Bianchi, T. Carey, L. Viti, L. Li, E.H. Linfield, A.G. Davies, A. Tredicucci, D. Yoon, P.G. Karagiannidis, L. Lombardi, F. Tomarchio, A.C. Ferrari, F. Torrisi, M. S. Vitiello, Terahertz saturable absorbers from liquid phase exfoliation of graphite, Nat. Commun. 8 (2017) 15763.
[20] D. Steinberg, R.M. Gerosa, F.N. Pellicer, J.D. Zapata, S.H. Domingues, E.A. Thoroh de Souza, L. Saito, Graphene oxide and reduced graphene oxide as saturable absorbers onto d-shaped fibers for sub 200fs EDFL mode locking, Opt. Mater. Express 8 (1) (2018) 144.
[21] Q. Bao, H. Zhang, Y. Wang, Z. Ni, Y. Yan, Z.X. Shen, K.P. Loh, D.Y. Tang, Atomic-layer graphene as a saturable absorber for ultrafast pulsed lasers, Adv. Funct. Mater. 19 (19) (2009) 3077–3083.
[22] F. Bonaccorso, Z. Sun, T. Hasan, A. Ferrari, Graphene photonics and optoelectronics, Nat. Photonics 4 (9) (2010) 611–622.
[23] D. Popa, Z. Sun, T. Hasan, F. Torrisi, F. Wang, A. Ferrari, Graphene Q-switched, tunable fiber laser, Appl. Phys. Lett. 98 (2011), 073106.
[24] E. Ugolotti, A. Schmidt, V. Petrov, J. Wan Kim, D.I. Yeom, F. Rotermund, S. Bae, B. Hee Hong, A. Agnesi, C. Fiebig, G. Erbert, X. Mateos, M. Aguiló, F. Diaz, U. Griebner, Graphene mode-locked femtosecond Yb: KLuW laser, Appl. Phys. Lett. 101 (16) (2012), 161112.
[25] M.S.A. Bhuyan, M.N. Uddin, M.M. Islam, F.A. Bipasha, S.S. Hossain, Synthesis of graphene, Int. Nano Lett. 6 (2016) 65–83.
[26] Y. Song, Carbon nanotube and graphene photonic devices, in: S. Yamashita, Y. Saito, J. Choi (Eds.), Carbon Nanotubes and Graphene for Photonic Applications, Woodhead Publishing Limited, Cambridge, 2013, pp. 48–84.
[27] A. Martinez, K. Fuse, S. Yamashita, Mechanical exfoliation of graphene for the passive mode-locking of fiber lasers, Appl. Phys. Lett. 99 (2011), 121107.
[28] D.B. Farmer, H.Y. Chiu, Y.M. Lin, K.A. Jenkins, F. Xia, P. Avouris, Utilization of a buffered dielectric to achieve high field-effect carrier mobility in graphene transistors, Nano Lett. 9 (12) (2009) 4474–4478.

[29] G. Sobon, J. Sotor, J. Jagiello, R. Kozinski, M. Zdrojek, M. Holdynski, P. Paletko, J. Boguslawski, L. Lipinska, K.M. Abramski, Graphene oxide vs. reduced graphene oxide as saturable absorbers for Er-doped passively mode-locked fiber laser, Opt. Express 20 (17) (2012) 19463–19473.
[30] X.F. Wang, J.H. Zhang, Z.Y. Gao, G.Q. Xia, Z.M. Wu, Nanosecond mode-locked Tm-doped fiber laser based on graphene saturable absorber, Acta Phys. Sin. 66 (11) (2017), 114209.
[31] H.X. Tsao, C.H. Chang, S.T. Lim, J.K. Sheu, T.Y. Tsai, Passively gain-switched and self mode-locked thulium fiber laser at 1950 nm, Opt. Laser Technol. 56 (2014) 354–357.
[32] H. Ahmad, R. Ramli, H. Monajemi, S.A. Reduan, N. Yusoff, M.F. Ismail, Soliton mode-locking in thulium-doped fibre laser by evanescent field interaction with reduced graphene oxide-titanium dioxide saturable absorber, Laser Phys. Lett. 16 (7) (2019), 075102.
[33] M. Wang, Y. Huang, Z. Song, J. Wei, J. Pei, S. Ruan, Two-micron all-fiberized passively mode-locked fiber lasers with high-energy nanosecond pulse, High. Power Laser Sci. Eng. 8 (2020) 1–8.
[34] A.S. Sharbirin, M.Z. Samion, M.F. Ismail, H. Ahmad, Ultrafast mode-locked dual-wavelength thulium-doped fiber laser using Mach-Zehnder interferometric filter, Opto Electron. Rev. 26 (2018) 312–316.
[35] H. Ahmad, M.Z. Samion, A.S. Sharbirin, S.F. Norian, S.N. Aidit, M.F. Ismail, Graphene-PVA saturable absorber for generation of a wavelength-tunable passively Q-switched thulium-doped fiber laser in 2.0 μm, Laser Phys. 28 (5) (2018), 055105.
[36] M.F.A. Rahman, A.A. Latiff, U.Z.M. Zaidi, M.F.M. Rusdi, A.H.A. Rosol, A.R. Bushroa, K. Dimyati, S.W. Harun, Q-switched and mode-locked thulium-doped fiber laser with pure antimony film saturable absorber, Opt. Commun. 421 (2018) 99–104.
[37] A.R. Muhammad, M.T. Ahmad, R. Zakaria, P.P. Yupapin, S.W. Harun, M. Yasin, Mode-locked thulium doped fibre laser with copper thin film saturable absorber, J. Mod. Opt. 66 (13) (2019) 1381–1385.
[38] A.S. Al-Hiti, A.H.H. Al-masoodi, H. Arof, W.R. Wong, S.W. Harun, Tungsten tri-oxide (WO_3) film absorber for generating Q-switched pulses in erbium laser, J. Mod. Opt. 67 (4) (2020) 374–382.
[39] M. Park, H. Kim, J.P. Youngblood, S.W. Han, E. Verplogen, A.J. Hart, Excellent dispersion of MWCNTs in PEO polymer achieved through a simple and potentially cost-effective evaporation casting, Nanotechnology 22 (2011), 415703.
[40] G. Sobon, J. Sotor, I. Pasternak, A. Krajewska, W. Strupinski, K.M. Abramski, Thulium-doped all-fiber laser mode-locked by CVD-graphene/PMMA saturable absorber, Opt. Express 21 (10) (2013) 12797.
[41] T. Hasan, V. Scardaci, P.H. Tan, F. Bonaccorso, A.G. Rozhin, Z. Sun, A.C. Ferrari, Nanotube and graphene polymer composites for photonics ad optoelectronics, in: A.C. Ferrari (Ed.), Molecular and Nanotubes, Springer Science, Cambridge, 2011, pp. 304–307.
[42] I.M. Babar, M.C. Paul, S. Das, A. Dhar, H. Ahmad, S.W. Harun, Mode-locked thulium ytterbium co-doped fiber laser with graphene saturable absorber, Photonics Lett. Pol. 8 (4) (2016) 104–106.
[43] M. Zhang, E.J.R. Kelleher, F. Torrisi, Z. Sun, T. Hasan, D. Popa, F. Wang, A.C. Ferrari, S.V. Popov, J.R. Taylor, Tm-doped fiber laser mode-locked by graphene polymer composite, Opt. Express 20 (2012) 25077–25084.
[44] B.K. Park, M.M. Kim, Applications of chitin and its derivatives in biological medicine, Int. J. Mol. Sci. 11 (2010) 5152–5164.
[45] Z. Song, G. Li, F. Guan, W. Liu, Application of chitin/chitosan and their derivatives in the papermaking industry, Polymers 10 (2018) 389.
[46] Z. Shervani, Chitin-gold nanocomposite film and electro-optical properties, Front. Nanosci. Nanotechnol. 3 (3) (2017) 2–4.
[47] N. Kokalis Burelle, Chitin amendments for suppression of plant nematodes and fungal pathogens, Phytopathology 91 (2001) 5168–5175.
[48] R.A.A. Muzzarelli, O. Tubertini, Chitin and chitosan as chromatographic supports and adsorbents for from organic and aqueous solutions and seawater, Talanta 16 (1969) 1571–1577.
[49] R. Jayakumar, V.V. Divya Rani, K.T. Shalumon, P.T. Sudheesh Kumar, S.V. Nair, T. Furuike, Bioactive and osteoblast cell attachment studies of novel α and β-chitin membranes for tissue engineering applications, Int J. Biol. Macromol. 45 (2009) 260–264.
[50] S.N.F. Zuikafly, W.M.F. Nawawi, L.H. Ngee, H. Yahaya, W.J. Yahya, F. Ahmad, Graphene in chitin based passive Q-switcher, J. Phys. Conf. Ser. 1371 (2019), 012011.
[51] W.M.F. Wan Nawawi, K.Y. Lee, E. Kontturi, R.J. Murphy, A. Bismarck, Chitin nanopaper from mushroom extract: natural composite of nanofibers and glucan from a single biobased source, ACS Sustain. Chem. Eng. 7 (7) (2019) 6492–6496.
[52] L. Escobar-Alarcon, M.E. Espinosa-Pesqueira, D.A. Solis-Casados, J. Gonzalo, J. Solis, M. Martinez-Orts, E. Haro-Poniatowski, Two-dimensional carbon nanostructures obtained by laser ablation in liquid: effect of an ultrasonic field, Appl. Phys. A 124 (2018) 141.
[53] S. Perumbilavil, P. Sankar, P.R. Thankamani, R. Philip, White light Z-scan measurements of ultrafast optical nonlinearity in reduced graphene oxide nanosheets in the 400–700 nm region, Appl. Phys. Lett. 107 (2015), 051104.
[54] S.I. Azzam, A.V. Kildishev, Time-domain dynamics of saturation of absorption using multilevel atomic systems, Opt. Mater. Express 8 (12) (2018) 3829–3834.
[55] L. Li, R.D. Lu, S.C. Liu, Z.D. Chen, J. Wang, Y.G. Wang, W. Ren, Using reduced graphene oxide to generate Q-switched pulses in er-doped fiber laser, Chin. Phys. Lett. 35 (11) (2018), 114202.
[56] X. Jiang, S. Gross, M.J. Withford, H. Zhang, D.I. Yeom, F. Rottermund, A. Fuerbach, Low-dimensional nanomaterial saturable absorbers for ultrashort-pulsed waveguide lasers, Opt. Mater. Express 8 (10) (2018) 3055.
[57] H. Ahmad, S.A. Reduan, N.E. Ruslan, C.S.J. Lee, M.Z. Zulkifli, K. Thambiratnam, Tunable Q-switched erbium-doped fiber laser in the C-band region using nanoparticles (TiO2), Optics Commun. (2019).
[58] Z. Sun, T. Hasan, A.C. Ferrari, Ultrafast lasers mode-locked by nanotubes and graphene, Phys. E 44 (2012) 1082–1091.
[59] Z. Ciplak, N. Yildiz, A. Calimli, Investigation of graphene/Ag nanocomposites synthesis parameters for two different synthesis methods, Fuller., Nanotub. Carbon Nanostruct. 23 (2014) 361–370.
[60] K.Y. Lau, N.H. Zainol Abidin, M.H. Abu Bakar, A.A. Latif, F.D. Muhammad, N.M. Huang, M.F. Omar, M.A. Mahdi, Passively mode-locked ultrashort pulse fiber laser incorporating multi-layered graphene nanoplatelets saturable absorber, J. Phys. Commun. 2 (2018), 075005.
[61] D.J. Richardson, J. Nilsson, W.A. Clarkson, High power fiber lasers: current status and future perspectives, J. Opt. Soc. Am. B Opt. Phys. 27 (2010) B63–B92.
[62] D.Y. Shen, J.K. Sahu, W.A. Clarkson, High power widely tunable Tm:fibre lasers pumped by an Er, Yb co-doped fibre laser at 1.6 μm, Opt. Express 14 (2006) 6084–6090.
[63] A.S. Sharbirin, M.Z. Samion, M.F. Ismail, H. Ahmad, Ultrafast mode-locked dual-wavelength thulium-doped fiebr laser using a Mach-Zehnder interferometric filter, Opto Electron. Rev. 26 (2018) 312–316.
[64] R. Paschotta, Field Guide to Laser Pulse Generation, SPIE, Washington, USA, 2008.
[65] G.R. Lin, I.H. Chiu, M.C. Wu, 1.2 ps mode-locked semiconductor optical amplifier fiber laser pulses generated by 60 ps backward dark-optical comb injection and soliton compression, Opt. Express 13 (3) (2005) 1008–1014.
[66] Y.H. Lin, G.R. Lin, Kelly sideband variation and self-four-wave-mixing in femtosecond fiber soliton laser mode-locked by multiple exfoliated graphite nano-particles, Laser Phys. Lett. 10 (4) (2013), 045109.
[67] Y. Wang, S. Fu, X. Tang, J. Kong, J.H. Lee, L. Zhao, Soliton distillation of pulses from a fiber laser, J. Light. Technol. 39 (8) (2021) 2542–2546.
[68] R. Weill, A. Bekker, V. Smulakovsky, B. Fischer, Spectral sidebands and multi-pulse formation in passively mode-locked lasers, Phys. Rev. A 83 (2011), 043831.
[69] Y. Wang, S. Wang, J. Luo, Y. Ge, L. Li, D. Tang, D. Shen, S. Zhang, F.W. Wise, L. Zhao, Vector soliton in a Tm fiber laser, IEEE Photonics Technol. Lett. 26 (8) (2014) 769–772.
[70] C.C. Hsu, J.H. Lin, W.F. Hsieh, Pulse train modulation in a picosecond self-mode-locked laser, J. Phys. B Mol. Opt. Phys. 42 (14) (2009), 145402.
[71] T. Kolokolnikov, S. Bielawski, The Q-switching instability in passively mode-locked lasers, Phys. D 219 (2006) 13–21.
[72] C. Honninger, R. Paschotta, F. Morier-Genoud, M. Moser, U. Keller, Q-switching stability limits of continuous-wave passive mode locking, J. Opt. Soc. Am. B 16 (1) (1999) 46–56.
[73] G. Yang, Y.G. Liu, Z. Wang, J. Lou, Z. Wang, Z. Liu, Broadband wavelength tunable mode-locked thulium-doped fiber laser operating in the 2μm region by using a graphene saturable absorber on microfiber, Laser Phys. Lett. 13 (2016), 065105.

[74] H.X. Tsao, C.H. Chang, S.T. Lim, J.K. Sheu, T.Y. Tsai, Passively gain-switched and self mode-locked thulium fiber laser at 1950 nm, Opt. Laser Technol. 56 (2014) 354–357.
[75] Q. Wang, T. Chen, B. Zhang, M.S. Li, Y.F. Lu, K. Cen, All-fiber passively mode-locked thulium-doped fiber ring laser using optically deposited graphene saturable absorbers, Appl. Phys. Lett. 102 (2013), 131117.
[76] S.A. Sadeq, S.W. Harun, A.H. Al-Janabi, Ultrahsort pulse generation with an erbium-doped fiber laser ring cavity based on a copper oxide saturable absorber, Appl. Opt. 57 (18) (2018) 5180–5185.
[77] J. Wang, X. Wang, J. Lei, M. Ma, C. Wang, Y. Ge, Z. Wei, Recent advances in mode-locked fiber lasers based on two-dimensional materials, Nanophotonics 9 (8) (2020) 2315–2340.
[78] H. Ahmad, R. Ramli, H. Monajemi, S.A. Reduan, N. Yusoff, M.F. Ismail, Soliton mode-locking in thulium-doped fibre laser by evanescent field interaction with reduced graphene oxide-titanium dioxide saturable absorber, Laser Phys. Lett. 16 (7) (2019), 075102.
[79] R. Zhang, X. Li, S. Dai, J. Li, L. Cao, D. Wu, S. Dai, J. Peng, J. Weng, Q.H. Nie, All-fiber 2 μm mode-locked thulium-doped fiber laser with the graphene oxide film, Optik 157 (2018) 1292–1299.
[80] X.F. Wang, J.H. Zhang, X.L. Peng, X.F. Ma, Generation and evolution of multiple operation states in passively mode-locked thulium-doped fiber laser by using a graphene-covered-microfiber, Chin. Phys. B 27 (8) (2018), 084215.
[81] Handbook of Graphene, Volume 3, Graphene-like 2D Materials M. Zhang Scrivener Publishing USA.